21st Australasian Fluid Mechanics Conference
Adelaide, Australia
10-13 December 2018

Dynamic Analysis of Myocardial Bridging: Impact of Heart Compression Force on Fractional Flow Reserve

J. Yi[1], F.B. Tian[2] and T. Barber[1]

[1]School of Mechanical & Manufacturing Engineering
University of New South Wales, Sydney, NSW 2052, Australia

[2]School of Engineering & Information Technology
University of New South Wales, Canberra, ACT 2612, Australia

Abstract

Myocardial bridging (MB) is an arterial disease and presents as a dynamic stenosis where in systole the artery is squeezed due to the heart contraction, while in diastole it remains uncompressed and normal. The prevalence of MB is high on autopsy cases and functional MB may lead to coronary syndromes or even the sudden cardiac death. Fractional flow reserve (FFR) has been proposed to evaluate the severity of coronary stenosis, including in cases of MB, and is the gold standard in clinic. FFR is simplified as a ratio of two pressures trans-stenosis in hyperemia, and is a unitless index ranging from 0 to 1. The cut-off value is 0.75 and if measured FFR is less than this, further intervention may be considered. The main objective of this research is to explore the impact of the heart compression force in systole on FFR using the fluid-structure interaction (FSI) study. The blood flow is assumed to be incompressible and Newtonian, and the vessel wall is assumed to be linear elastic. A force function was applied in solid domain and the length of force region was varied, in terms of 1D (Diameter, mm), 4D, 8D, 12D, 16D, 20D. The distributions of the blood flow velocity, the vessel wall stress and the pressure are presented. The results showed that the value of FFR was slightly reduced with the increase of force range.

Introduction

Epicardial coronary artery underlying the muscle is termed as myocardial bridging (MB). MB is a congenital disease and on average is present in one third of adults [5]. MB is observed as many as 40% to 80% of cases on autopsy and mainly occurs in the middle of the left anterior descending coronary artery (LAD) [3]. In systole, the vessel is compressed due to the heart contraction, while in diastole it remains uncompressed and normal. MB is a dynamic stenosis and the length of the bridging is one of the main factors contributing to the occurrence of myocardial ischemia [1].

In clinical diagnosis, vessel anatomy is frequently used for disease identification and percent diameter stenosis (DS%) provides a simple yet appropriate metric of lesions. DS% is typically calculated as the difference between the minimal luminal diameter (MLD) and the target reference vessel diameter (RVD), divided by RVD and multiplied by 100 to get the percentage of stenosis. Based on the definition, DS% would be the same if two cases have the same MLD and RVD but different lesion length, which indicates that DS% does not include much effect of the length of the stenosis.

Fractional flow reserve (FFR) was proposed [6] to more accurately evaluate the functional severity of coronary stenosis. And FFR-guided percutaneous coronary intervention (PCI) may bring about better clinical outcomes compared with angiography-based therapy [4, 9]. FFR is defined as the ratio of the flow in stenotic artery to the flow in the same artery in the hypothetical case that the stenosis were removed in hyperemia condition. Due to the applicability and accessibility in clinic, FFR is simplified as a ratio of the distal pressure (P_d) to the aorta pressure (P_a) [2].

In this research, a force function was created to mimic the heart compression force in systole, and different lengths of force region were applied to investigate their effects on MB. FFR was used as an evaluation method of MB and a smaller value indicates that the disease is more severe.

Method

The simulations were performed in the commercial software of COMSOL Multiphysics 5.3 based on finite element method (FEM). A "2D Asymmetric" component was selected with polar coordinates (r, z). Two rectangles were built and by revolving the plane along z axis, the three-dimensional geometry was constructed automatically (figure 1). The diameter (D) of the vessel is 3 mm and the wall thickness is 0.5 mm.

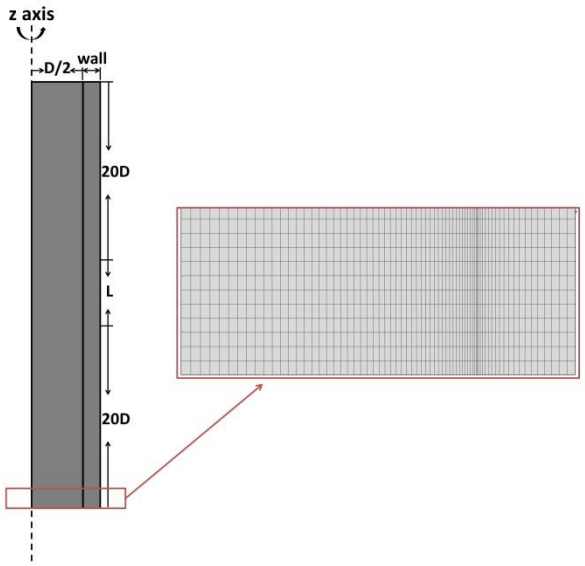

Figure 1. Schematic illustration of the ideal model. L denotes the length of the force region applied in the vessel wall. The lengths of entering and exiting the compression part are both 20D. The block diagram in red colour presents the meshing of the computed model.

The studies of the fluid-solid interaction (FSI) were employed. The incompressible flow of a Newtonian fluid in steady state is governed by the continuity and Navier-Stokes equations, respectively:

$$\nabla \cdot \boldsymbol{u_f} = 0 \tag{1}$$

and

$$\rho_f \boldsymbol{u_f} \cdot \nabla \boldsymbol{u_f} - \nabla \cdot \boldsymbol{\sigma_f} = 0 \tag{2}$$

where u_f is the fluid velocity vector, ρ_f is the density of the fluid and σ_f is the stress tensor of the fluid. The motion of the structure is described by:

$$-\nabla \cdot \boldsymbol{\sigma_s} = \rho_s \boldsymbol{f_s} \quad (3)$$

where σ_s represents the stress tensor of the solid, ρ_s represents the density of the solid and f_s represents the load applied on the structure. At the FSI interface, the fluid and solid velocities are equal based on kinematic coupling equation:

$$\boldsymbol{u_f} = \frac{\partial \xi_s}{\partial t} \quad (4)$$

where ξ_s represents the displacement of the solid. And the normal stresses are opposite based on the dynamic coupling equation:

$$\boldsymbol{\sigma_f} \cdot \boldsymbol{n_f} = \boldsymbol{\sigma_s} \cdot \boldsymbol{n_s} \quad (5)$$

where n_f and n_s are the unit vectors normal to the interface inwards from the fluid and solid side.

The flow was set as laminar with a density of 1050 kg/m^3 and a dynamic viscosity of 0.00365 Pa·s. The material of the solid domain was linear elastic. The Young's modulus of it is 3×10^6 Pa and the Poisson's ratio is 0.3. The density of the arterial wall was defined as 1150 kg/m^3 as well.

The discretization of the geometry was based on "Mapped" scheme. The nodes were distributed by prescribing different numbers and element ratios along the edges of the model. The quad meshing was generated and the elements close to the FSI interface were refined and optimized (figure 1). The quality of the meshing ranges from 0.9 to 1 in all of the computed models. And the deformation of the meshing in the computation was set as "Winslow" smoothing type.

The pressure of 100 mmHg was applied at the inlet, and the normal outflow velocity of 0.4 m/s was applied at the outlet. A force function was generated [7] and was applied in the solid domain (equation (6)). The "Direct" and "Segregated" scheme were used in the stationary solver.

$$f(z) = 200 \times e^{\frac{-4\times z^2}{(\frac{L}{2})^2}} \quad (-\frac{L}{2} \le z \le \frac{L}{2}) \quad (6)$$

Numerical models with different values of L were studied, 1D, 4D, 8D, 12D, 16D and 20D respectively. FFR was calculated by the ratio of P_d/P_a, where P_d was obtained at the central point of the plane 10D down the narrowing [8], while P_a was obtained at the central point of the plane of the inlet.

Results and Discussion

The stability and accuracy of the simulations were analysed in the six models. P_d is a significant parameter and was chosen for the convergence study. The results of the tolerance analysis of the model with L of 8D are presented in table 1. The tolerance was set as 1×10^{-3}, 1×10^{-4}, 1×10^{-5}, and 1×10^{-6}. However, the value of P_d remained the same as 1.2689×10^4 Pa. Therefore, the tolerance of the simulation was defined as the default number of 1×10^{-3}.

Tolerance Level	P_d (Pa)
1×10^{-3}	1.2689×10^4
1×10^{-4}	1.2689×10^4
1×10^{-5}	1.2689×10^4
1×10^{-6}	1.2689×10^4

Table 1. The convergence study of the tolerance level in the model with L of 8D.

Different meshing sizes were created, in terms of 5×10^4, 1×10^5, 2×10^5 and 4×10^5. Similarly, table 2 shows the meshing convergence study of the model with L of 8D. The variable of P_d was selected and the values in different meshing size were compared. According to the results, the increasing of the mesh size did not affect the outcomes of P_d. The main difference and the grid convergence index (GCI) are both zero. Therefore, the meshing with 5×10^4 elements was selected to compute the convergent results.

Meshing Size	P_d (Pa)
5×10^4	1.2689×10^4
1×10^5	1.2689×10^4
2×10^5	1.2689×10^4
4×10^5	1.2689×10^4

Table 2. The convergence study of the meshing size in the model with L of 8D.

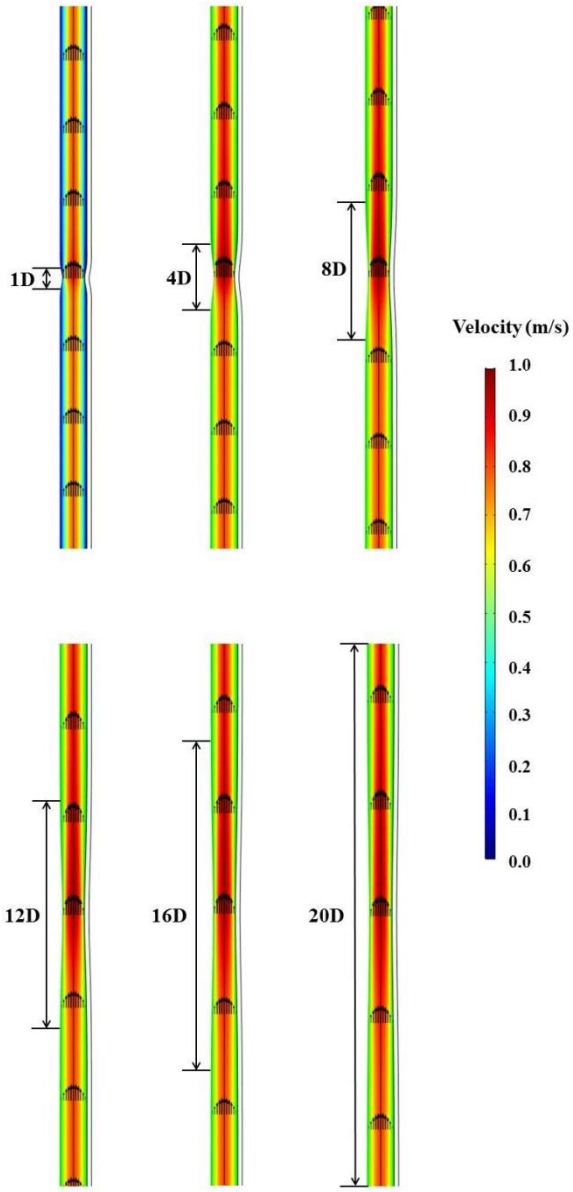

Figure 2. Velocity contours of the central cut-plane. The height presented is only 20D in the middle of the entire model. The arrows in black represent the flow direction.

The ideal artery model is compressed and the stenosis of the models with different L are shown (figure 2). The velocity contour of a cut-plane was drawn and the maximal velocity of the six models is around 1 m/s. If the value of L is too small, like 1D, the velocity in the position of $\frac{3}{4}$D is close to 0.1 m/s. However, when the value of L increases, the magnitude of velocity in that place is about 0.5 m/s.

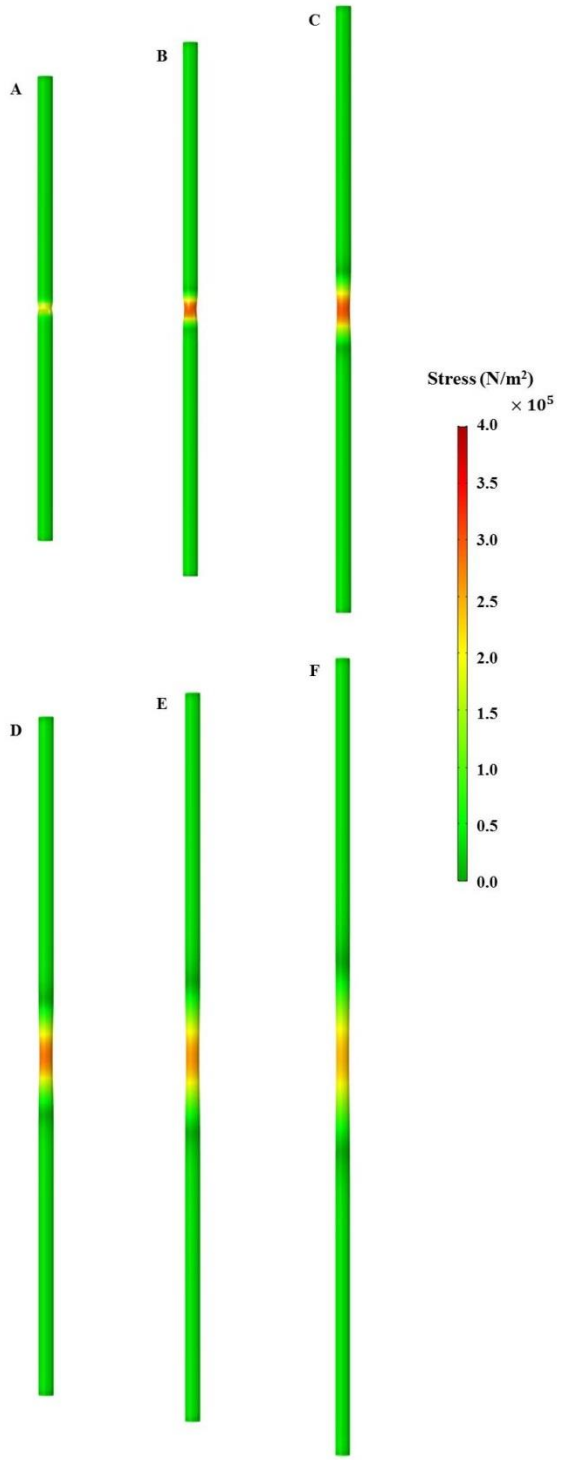

Figure 3. Von Mises Stress distributions of the arterial wall. A to F represent the model with L of 1D, 4D, 8D, 12D, 16D, 20D, respectively.

The region of the large value of the von Mises stress mainly distributes near the compression part (figure 3). The magnitude of the stress in the entry and exit region is around 0.5×10^5 N/m^2. In addition, with the increase of L, the maximal value of the stress is reduced, from 5.7×10^5, 4.9×10^5, 4.0×10^5, 3.7×10^5, and 3.5×10^5, to 3.2×10^5 N/m^2 (table 3).

L of The Model	Maximal Value of Stress (N/m^2)
1D	5.7×10^5
4D	4.9×10^5
8D	4.0×10^5
12D	3.7×10^5
16D	3.5×10^5
20D	3.2×10^5

Table 3. The maximal value of the von Mises stress of the solid domain in the six models.

Generally, the pressure contours of the six models dose not show much difference (figure 4). However, if the lesion length of the stenosis is very small, the value of pressure jumped more rapidly than the case with a larger L. The value of P_d is decreased if the value of L increases, in terms of 1.2861×10^4, 1.2766×10^4, 1.2689×10^4, 1.2619×10^4, 1.2552×10^4, and 1.2486×10^4 Pa (table 4). Therefore, FFR values were slightly decreased, from 0.96 to 0.94. Clinically, the value of FFR detected in the patients may be less than 0.75. Results in the simulations with the FFR value larger than 0.9 may be because of the amplitude of the force.

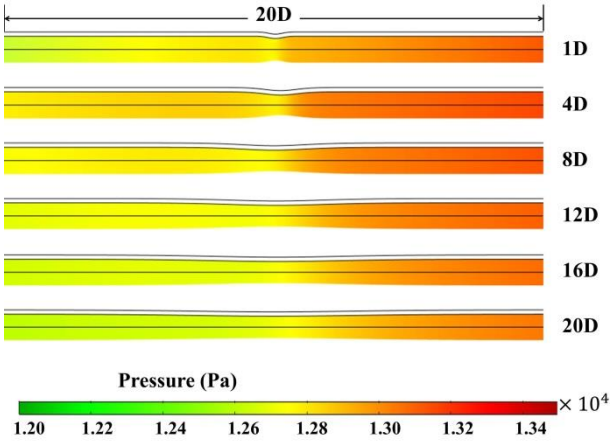

Figure 4. Pressure distributions of the numerical models. The length of the presented contours is only 20D in the middle of the entire model.

L of The Model	P_d (Pa)	FFR	DS%
1D	1.2861×10^4	0.96	15
4D	1.2766×10^4	0.96	23
8D	1.2689×10^4	0.95	20
12D	1.2619×10^4	0.95	18
16D	1.2552×10^4	0.94	16
20D	1.2486×10^4	0.94	14

Table 4. The results of FFR and DS% of the six models in different value of L.

The results of the DS% are shown in table 4 as well. If the DS% is chosen as the evaluation tool, according to the definition, the severest case of the six models is the second one of 23% narrowing. However, if choosing FFR as the

assessment tool, the severest case is the last model. That may further imply the inconsistency of using different methods to evaluate MB.

Conclusion

FSI studies of the ideal MB models were analysed in the commercial software and the impact of the length of compression force region on FFR was identified. The contours of the flow velocity, the von Mises stress and the pressure were presented as well. It was found that FFR value was slightly decreased if the force region enlarged.

Limitations and Future Work

There are several limitations of this study. Firstly, an ideal cylinder model was simulated rather than the patient-specific case. Clinically, the artery of the patient may be highly tortuous and the haemodynamic research of that may show different outcomes. Secondly, the simulation is in steady state. However, MB is a dynamic stenosis and the characteristics in systole and diastole are varied, which implies that a transient study would reveal more of the mechanism of the disease. Thirdly, the deformation of the FSI model is not very large and a more severe case may be constructed in the future.

The experimental study and data from the hospital would be used to validate the computational results in the future as well. At present, the bridging rig has been built mimicking the morphology of MB and measurements of FFR have been performed in the laboratory.

References

[1] Bourassa, M.G., Butnaru, A., Lespérance, J. & Tardif, J.C., Symptomatic Myocardial Bridges: Overview of Ischemic Mechanisms and Current Diagnostic and Treatment Strategies, *Journal of the American College of Cardiology*, **41**, 2003, 351-359.

[2] Bruyne, B.D. & Sarma, J., Fractional Flow Reserve: A Review, *Heart*, **94**, 2008, 949-959.

[3] Corban, M.T., Hung O.Y., Eshtehardi, P., Rasoul-Arzrumly, E., McDaniel, M., Mekonnen, G., Timmins, L.H., Lutz, J., Guyton, R.A. & Samady, H., Myocardial Bridging: Contemporary Understanding of Pathophysiology with Implications for Diagnostic and Therapeutic Strategies, *J Am Coll Cardiol*, **63**, 2014, 2346-2355.

[4] De Bruyne, B., Pijls, N.H., Kalesan, B., Barbato, E., Tonino, P.A., Piroth, Z., Jagic, N., Mobius-Winkler, S., Rioufol, G., Witt, N., Kala P., MacCarthy, P., Engstrom, T., Oldroyd, K.G., Mavromatis, K., Manoharan, G., Verlee, P., Frobert, O., Curzen, N., Johnson, J.B., Juni, P. & Fearon, W.F., Fractional Flow Reserve-Guided PCI versus Medical Therapy in Stable Coronary Disease, *N Engl J Med*, **367**, 2012, 991-1001.

[5] Mohlenkamp, S, Update on Myocardial Bridging, *Circulation*, **106**, 2002, 2616-2622.

[6] Pijls, N.H.J., Son, J.A.v, Richard, L.K., Bernard, D.B. & Gould, K.L, Experimental Basis of Determining Maximum Coronary, Myocardial, and Collateral Blood Flow by Pressure Measurements for Assessing Functional Stenosis Severity Before and After Percutaneous Transluminal Coronary Angioplasty, *Circulation*, **87**, 1993, 1354-1367.

[7] Siouffi, M., Deplano, V. & Pelissier, R., Experimental Analysis of Unsteady Flows Through A Stenosis, *J Biomech*, **31**, 1998, 11-19.

[8] Solecki, M., Kruk, M., Demkow, M., Schoepf, U.J., Reynolds, M.A., Wardziak, L., Dzielinska, Z., Spiewak, M., Milosz-Wieczorek, B., Malek, L., Marczak, M. & Kepka, C., What Is The Optimal Anatomic Location for Coronary Artery Pressure Measurement at CT-Derived FFR?, *J Cardiovasc Comput Tomogr*, **11**, 2017, 397-403.

[9] Tonino, P.A.L., Bruyne, B.D., Pijls, N.H.J., Siebert, U., Ikeno, F., Veer, M.v., Klauss, V., Manoharan, G., Engstrom, T., Oldroyd, K.G., Lee, P.N.V., MacCarthy, P.A. & Fearon, W.F., Fractional Flow Reserve versus Angiography for Guiding Percutaneous Coronary Intervention, *The New England Journal of Medicine*, **360**, 2009, 213-224.